

# Solid Circulation Rate in a Continuous CO<sub>2</sub> Absorption Fluidized Bed Reactor

Daoyin LIU and Xiaoping CHEN

*Key Laboratory of Energy Thermal Conversion and Control of Ministry of Education,  
School of Energy and Environment, Southeast University, Nanjing 210096, Jiangsu, China*

**Keywords:** Fluidized Bed Reactor, CO<sub>2</sub> Capture, Sodium Carbonate, Potassium Carbonate, Solid Circulation Rate

A new CO<sub>2</sub> absorption fluidized bed reactor is presented for a continuous CO<sub>2</sub> capture process using sodium- or potassium-based solid sorbents. The absorption reactor includes a bubbling bed and a narrowed upper riser, which are connected by using a combination of a central tube and a draft tube. The control of solid circulation is demonstrated by a cold model. Effects on the solid circulation rate ( $G_s$ ) of various parameters are investigated, including the geometry parameters (the position of the central tube exit, and the draft tube diameter), the operating parameters (gas velocity in the draft tube and the annular zone, the static bed material height, and the particle size). Finally, an expression is derived to correlate  $G_s$  as a function of the particle properties and operating conditions.

## Introduction

The fluidized bed reaction using sodium- or potassium-based solid sorbents is one of the most promising technologies for post-combustion CO<sub>2</sub> capture from the flue gas of fossil fuel plants, which has advantages of low corrosion compared to absorption processes using liquid solution (Lee *et al.*, 2006; Wang *et al.*, 2011; Zhao *et al.*, 2013). Such a process usually includes two reactors: an absorption reactor and regeneration reactor. In the absorption reactor, CO<sub>2</sub> reacts with the sorbent particles of sodium carbonate (Na<sub>2</sub>CO<sub>3</sub>) or potassium carbonate (K<sub>2</sub>CO<sub>3</sub>). The reacted sorbents (NaHCO<sub>3</sub> or KHCO<sub>3</sub>) are then transported into the regeneration reactor, where the decomposition reaction takes place, yielding the regenerated sorbents (Na<sub>2</sub>CO<sub>3</sub> or K<sub>2</sub>CO<sub>3</sub>) and CO<sub>2</sub>. The regenerated sorbents are then transported to the absorption reactor again and absorb CO<sub>2</sub>.

Effective controlling of solid flow between the two reactors is critical for realizing a continuous CO<sub>2</sub> capture process, which is also recognized as a challenge in other similar carbonator-looping systems. To achieve this aim, several typical systems consisting of dual fluidized bed reactors have been developed so far. One type is a dual bubbling fluidized bed system (Ryu *et al.*, 2008). Fang *et al.* (2009) demonstrated continuous CO<sub>2</sub> capture using calcium-based sorbents in a dual bubbling fluidized bed system, where the solid flow between the two beds was realized by solid injection nozzles inserted into the dense fluidized beds. In our previous studies, we built a dual bubbling fluidized bed system with a flue gas treatment of  $\sim 10 \text{ Nm}^3/\text{h}$ , where the potassium-based sorbents between the two reactors are transported by screw

feeders. The solid flow can be well controlled, but it would be difficult to employ screw feeders in industrial scale reactors (Wu *et al.*, 2013). The dual bubbling fluidized bed system is not effective at handling particle transport at large scale. Another type is a system with a fast fluidized bed for absorption and a bubbling fluidized bed for regeneration, where the particle transport is controlled by gas velocity (Yi *et al.*, 2008). Park *et al.* (2011) demonstrated a pilot system using alkali metal based sorbents with a gas treatment of  $2,000 \text{ Nm}^3/\text{h}$ . Due to the successful control of solid circulation, the dual reactor system with a fast bed and a bubbling bed is applied more.

Based on multiphase reaction mechanisms, the CO<sub>2</sub> absorption reaction is a heterogeneous reaction which is highly affected by solid concentration (Levenspiel, 1998). Among typical types of fluidized bed reactors, the moving and fixed beds have the highest solid concentration, and the next is the bubbling fluidized bed, and the last is the fast bed. In the moving and fixed beds, the removal of the reaction heat could be a problem, while the bubbling fluidized bed reactor is almost isothermal because of its high heat and mass transfer rate.

Combination of the high solid concentration of the bubbling bed and the efficient capability of handling particle transport of the fast bed, we propose a new fluidized bed reactor for capturing CO<sub>2</sub> in a continuous absorption and regeneration process. Compared with the bubbling-fast bed system, it has a more compact design, while compared with the dual bubbling fluidized bed system, it is more efficient to transport particles. Generally, the new reactor includes a bubbling bed and a narrowed upper riser, which are connected by using a combination of a central tube and a draft tube. By adjusting the gas flow into the draft tube, the solid circulation rate can be effectively controlled. A cold model is constructed, and the effects of various parameters on the solid circulation rate are investigated and analyzed.

Received on May 22, 2015; accepted on March 24, 2016

DOI: 10.1252/jcej.15we124

Correspondence concerning this article should be addressed to D. Liu (E-mail address: dyliu@seu.edu.cn).

# 1. Experimental

## 1.1 Apparatus

A schematic of the cold model of the continuous fluidized bed reactor is shown in **Figure 1**. The reactor is proposed for post-combustion CO<sub>2</sub> capture using potassium based solid sorbents (Zhao *et al.*, 2013). The annular bed has high solid concentration which enables high efficiency of heterogeneous reaction, while the central and draft tubes enable the particle conveying in a controlled mode. It serves as an absorption reactor in the dual fluidized bed system. The cold model consisted of a main bed, cyclone, and loop-seal. The main bed coupled a bubbling fluidized bed and a narrowed upper riser. A central tube was inserted in the bubbling fluidized bed through its air distributor. To be clear, the bubbling bed is noted as an annular bed in the following. The gas velocity in the central tube was much higher than the annular bed, which entrains the particles into the draft tube. The draft tube connected with the upper riser. The particles were then transported upwards along the upper riser. Meanwhile, it should be noted that some particles can flow downwards from the upper riser to the annular bed through the clearance. The geometrical sizes of each section are listed in **Table 1**.

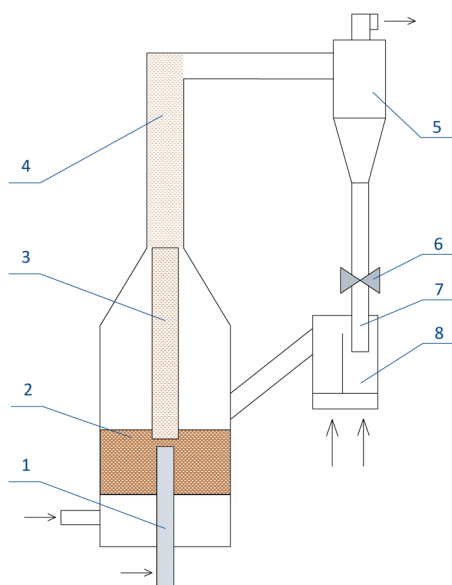


**Fig. 1** Schematic diagram of continuous fluidized bed reactor: 1, central tube; 2, annular bed; 3, draft tube; 4, upper riser; 5, cyclone; 6, ball valve; 7, return leg; 8, loop seal

**Table 1** Geometrical size of each section of the main bed

Sections	Inner diameter [m]	Height [m]
Central tube	0.033	—
Draft tube	0.04–0.08	1.17
Annular bed	0.2	1.2
Upper riser	0.1	0.5

## 1.2 Experimental conditions

The solid circulation rate ( $G_s$ ) was measured under various conditions. It is defined as the mass of particle flow per second through unit cross sectional area of the draft tube. By immediately turning off the ball valve installed in the return leg and measuring the height of the particles accumulated over a few seconds, the mass of particle flow is obtained. Then  $G_s$  is calculated by dividing the mass flow over the interval time and cross-sectional area of the draft tube. Two series of tests were conducted, where the geometrical parameters and the operating parameters were focused, respectively. In the first test series, the effects of the central tube exit position ( $z_c$ ) and the draft tube diameter ( $D_d$ ) on  $G_s$  were studied.  $z_c$  is defined as the distance between the top edge of the central tube and the bottom edge of the draft tube, and a negative value means the central tube is inserted into the draft tube. Sand particles with  $\rho_p = 2,620 \text{ kg/m}^3$  and  $d_p = 0.25\text{--}0.45 \text{ mm}$  were used as bed materials (sand I). The minimum fluidizing gas velocity ( $u_{mf}$ ) of sand I is 0.12 m/s determined by experiment, and terminal velocity ( $u_t$ ) is 2.8 m/s estimated by the classic correlation.

In the second test series, with the geometry fixed, the operating parameters were varied. Two sand particles were used, with  $d_p = 0.25\text{--}0.30 \text{ mm}$  (sand II) and  $0.35\text{--}0.45 \text{ mm}$  (sand III), whose  $u_{mf}$  were 0.08 and 0.16 m/s,  $u_t$  are 2.2 and 3.2 m/s, respectively. For each bed material, experiments were performed with different gas velocity in the draft tube ( $u_{g,d}$ ), gas velocity in the annular zone ( $u_{g,a}$ ), and static bed materials ( $h_0$ ). Please note that only the experimental data obtained in the second test series was used to correlate  $G_s$ .

## 2. Results

### 2.1 Influence of geometrical parameters

The variation of  $G_s$  with  $u_{g,d}$  under different  $z_c$  is shown in **Figure 2**.  $z_c$  is increased from  $-10$  to  $30 \text{ mm}$ , covering different relative positions between the central tube and the draft tube. Generally, it is shown that the effect of  $z_c$  on  $G_s$  is not strong. At lower draft gas velocities,  $G_s$  increases slightly as the central tube leaves the draft tube, because the flow port size between the central and draft tubes increases. Conversely, at higher draft velocities,  $G_s$  decreases slightly as the

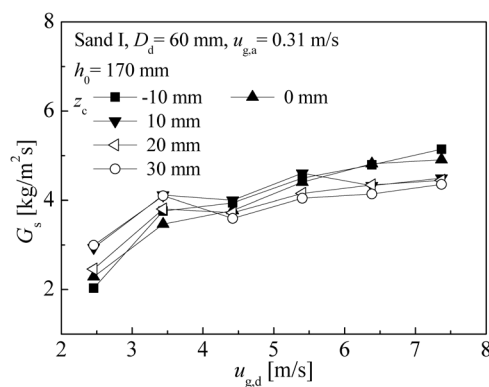


**Fig. 2**  $G_s$  variation with  $u_{g,d}$  under different  $z_c$

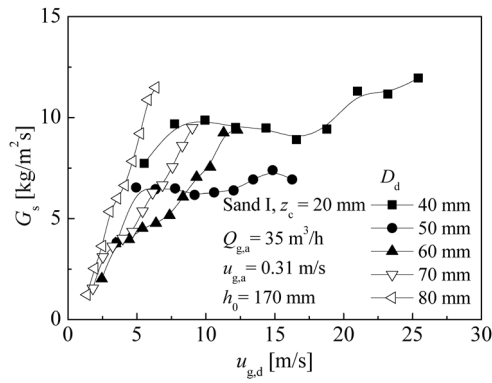


Fig. 3  $G_s$  variation with  $u_{g,d}$  under different  $D_d$

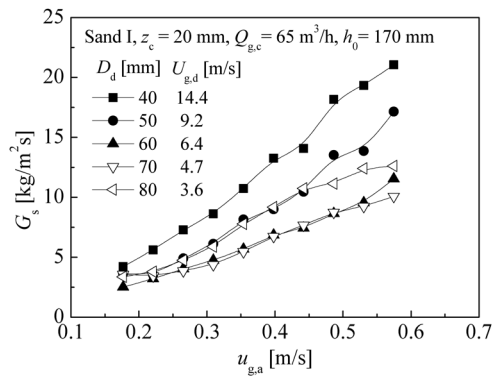


Fig. 4  $G_s$  variation with  $u_{g,a}$  under different  $D_d$ ; gas flow rate into the central tube ( $Q_{g,c}$ ) is fixed

central tube leaves the draft tube, because there is a risk of gas bypassing from the central tube to the annular bed when the gas velocity is high.

The variation of  $G_s$  with  $u_{g,d}$  under different  $D_d$  is shown in **Figure 3**.  $D_d$  is increased from 40 to 80 mm. Under large  $D_d$  of 60, 70, and 80 mm,  $G_s$  increases constantly with increasing the draft velocity. Under  $D_d = 80$  mm, the slope of increase in  $G_s$  with  $u_{g,d}$  is the largest. However, under small  $D_d$  of 40 mm and 50 mm, the increase of  $G_s$  is limited as the draft velocity increases. This is partly due to more gas bypassing to the annular bed under small draft tubes. Another important reason is that the clearance between the draft tube and upper riser increases as  $D_d$  decreases, which would increase the solids falling down from the upper riser through this clearance.

Furthermore, the variation of  $G_s$  with  $u_{g,a}$  under different  $D_d$  is shown in **Figure 4**. Under different  $D_d$ ,  $G_s$  increases steadily with  $u_{g,a}$ . This is because the bed expands more, leading more solids to be above the top of the central tube. With  $u_{g,a}$  fixed,  $G_s$  increases as  $D_d$  increases from 70 to 80 mm. This is further evidence that the clearance between the draft tube and upper riser can influence  $G_s$ . The clearance decreases with an increase in  $D_d$ , which would decrease the solids falling down from the upper riser through this clearance, promoting the increase of  $G_s$ .

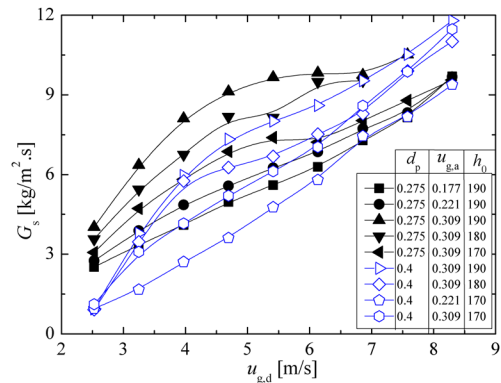


Fig. 5 Effect of  $u_{g,d}$  on  $G_s$  under conditions with different  $d_p$ ,  $u_{g,a}$ , and  $h_0$

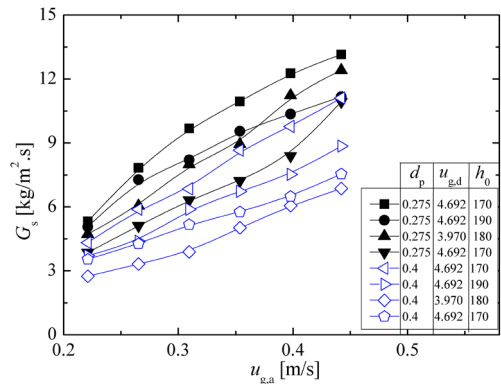


Fig. 6 Effect of  $u_{g,a}$  on  $G_s$  under conditions with different  $d_p$ ,  $u_{g,d}$ , and  $h_0$

## 2.2 Influence of operational parameters

In the following tests, the geometrical parameters are fixed with  $z_c = 20$  mm and  $D_d = 70$  mm. Two bed materials are tested, with the algorithmic average particle size of  $d_p = 0.275$  mm and 0.4 mm. For each bed material, different  $h_0$ ,  $u_{g,a}$ , and  $u_{g,d}$  are tested. In total, more than 110 runs are carried out.

**Figures 5 and 6** present a summary of  $G_s$  with a function of  $u_{g,d}$  and  $u_{g,a}$  under different conditions. It is shown that under all conditions,  $G_s$  increases almost linearly with both  $u_{g,d}$  and  $u_{g,a}$ . This is due to the fact that, by increasing  $u_{g,d}$ , more particles are carried up through the riser, and by increasing  $u_{g,a}$ , more particles are entrained from the annular zone to draft tube. In addition, it is seen that under the same velocity,  $G_s$  decreases with increasing  $d_p$  as expected.  $G_s$  increases with increasing  $h_0$ , because more particles are above the top of the central tube, leading more particles entrained from the annular zone to the draft tube.

## 3. Discussion

The solid circulation in the current fluidized bed depends on two processes: (a) particles are extracted from the annular zone to the draft tube; (b) particles are transported up through the riser. In the former process, as the gas flow

is injected from the central tube to the draft tube, a gas jet flow is formed. Solids close enough to the jet are entrained and carried up into the draft tube. Besides, the solids flowing from the annular zone into the draft tube is favored by the pressure difference, resulting from the loading of bed materials above the top of the central tube in the annular zone. Therefore, the solid flow rate is influenced by both the gas velocity in the central tube and the differential pressure between the annular bed and draft tube.

In the latter process, it is a fast fluidized process where the solid flow rate depends on the gas velocity and particle loading in the riser. However, it should be noted that, because the particles flow downwards mostly along the bed wall, some particles would flow downward from the upper riser to the annular bed through the clearance, which affects  $G_s$ , as presented in Figure 4. When correlating  $G_s$ , the effect of geometry is excluded. Thus,  $G_s$  is expressed as Eq. (1).

$$G_s = f(Ar, h_0 / h_c, u_{g,a} / u_{mf}, u_{g,d} / v_{p,t}) \quad (1)$$

Here,  $Ar$  is the particle Archimedes number,  $h_0$  static bed materials height, and  $v_{p,t}$  terminal velocity of a single particle. The data of the second test series, with the geometry fixed, are used to correlate  $G_s$ .

By means of nonlinear regression analysis using the results presented in Figures 5 and 6, the coefficient and exponents of each parameter are determined, as listed in Eq. (2),

$$G_s = 3.26 \times 10^{-4} Ar^{0.92} (h_0 / h_c)^{2.49} (u_{g,a} / u_{mf})^{1.18} (u_{g,d} / v_{p,t})^{1.39} \quad (2)$$

Figure 7 compares the measured  $G_s$  with the calculated values from Eq. (2). The agreement between them is acceptable, although the correlation does not fit all details. Equation (2) indicates the  $G_s$  can be controlled by the operating parameters of particle size, static bed height, and gas velocities in the annular and draft tubes. A correlation of  $G_s$  with the effect of geometry will be carried out in the future.

It has been shown in the above that the solid circulation rate can be controlled by different geometries and operating parameters. In principle, the reaction process which is heterogeneous and requires a continuous solid flow in and

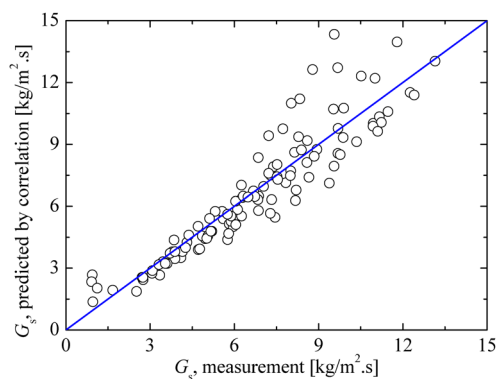


Fig. 7 Comparison between the measured and calculated values of  $G_s$

out of reactors, can also employ the present reactor. Compared to the dual bubbling fluidized bed system, the solid circulation rate can be controlled efficiently, which is an essential requirement of a continuous absorption-generation reaction process. Compared to a bubbling-fast bed system, the solid residence time in the present reactor can be longer, which makes the reactor more compact.

In this study, we have shown that the solid circulation rate depends strongly on the diameter of the draft tube, and gas velocities in the draft tube and annular bed. Since other factors, e.g., solid concentration and residence time distribution, can also have significant influence on  $\text{CO}_2$  absorption reaction, in the future, we will study the reactor performance under different parameters in a hot model.

## Conclusions

We present a new  $\text{CO}_2$  absorption fluidized bed reactor, for a continuous  $\text{CO}_2$  capture process using sodium- or potassium-based solid sorbents. It combines the advantage of high solid concentration of the bubbling bed and the advantage of good capability of handling particle transport of the fast bed.

Based on the cold model tests, the solid circulation rate depends rarely on the central tube exit position, but strongly on the draft tube diameter, and increases with increasing initial bed materials height, gas velocities in the annular bed and draft. Finally, the correlation of the solid circulation rate is derived as a function of the particle properties and operating conditions.

## Acknowledgement

We would like to acknowledge the financial support of this work by the National Natural Science Foundation of China (No. 51476030). We would like to thank Zhen Yang for assistance during construction of the experimental setup.

## Nomenclature

$Ar$	= particle Archimedes number	[—]
$d_p$	= particle diameter	[mm]
$D_d$	= draft tube diameter	[m]
$G_s$	= solid circulation rate	[kg/m <sup>2</sup> ·s]
$h_0$	= static bed materials height	[m]
$h_c$	= position of the central tube exit	[m]
$Q_{g,c}$	= gas flow rate to the central tube	[m <sup>3</sup> /h]
$u_{g,d}$	= gas velocity in the draft tube	[m/s]
$u_{g,a}$	= gas velocity in the annular zone	[m/s]
$u_{mf}$	= minimum fluidizing velocity	[m/s]
$v_{p,t}$	= terminal velocity of a single particle	[m/s]
$z_c$	= central tube position	[m]
$\varepsilon_s$	= solid volume fraction	[—]
$\rho_p$	= particle density	[kg/m <sup>3</sup> ]

## Literature Cited

Fang, F., Z. S. Li and N. S. Cai; "Continuous  $\text{CO}_2$  Capture from Flue Gases Using a Dual Fluidized Bed Reactor with Calcium-Based

- Sorbent," *Ind. Eng. Chem. Res.*, **48**, 11140–11147 (2009)
- Lee, S. C., B. Y. Choi, T. J. Lee, C. K. Ryu, Y. S. Soo and J. C. Kim; "CO<sub>2</sub> Absorption and Regeneration of Alkali Metal-Based Solid Sorbents," *Catal. Today*, **111**, 385–390 (2006)
- Levenspiel, O.; *Chemical Reaction Engineering*, 3rd ed., pp. 447–468, John Wiley and Sons, New York, U.S.A. (1998)
- Park, Y. C., S.-H. Jo, C. K. Ryu and C.-K. Yi; "Demonstration of Pilot Scale Carbon Dioxide Capture System Using Dry Regenerable Sorbents to the Real Coal-Fired Power Plant in Korea," *Energy Procedia*, **4**, 1508–1512 (2011)
- Ryu, H. J., Y. C. Park, S. H. Jo and M. H. Park; "Development of Novel Two-interconnected Fluidized Bed System," *Korean J. Chem. Eng.*, **25**, 1178–1183 (2008)
- Wang, S. P., S. L. Yan, X. B. Ma and J. L. Gong; "Recent Advances in Capture of Carbon Dioxide Using Alkali-Metal-Based Oxides," *Energy Environ. Sci.*, **4**, 3805–3819 (2011)
- Wu, Y., X. P. Chen, W. Dong, C. W. Zhao, Z. L. Zhang, D. Y. Liu and C. Liang; "K<sub>2</sub>CO<sub>3</sub>/Al<sub>2</sub>O<sub>3</sub> for Capturing CO<sub>2</sub> in Flue Gas from Power Plants. Part 5: Carbonation and Failure Behavior of K<sub>2</sub>CO<sub>3</sub>/Al<sub>2</sub>O<sub>3</sub> in the Continuous CO<sub>2</sub> Sorption-Desorption System," *Energy Fuels*, **27**, 4804–4809 (2013)
- Yi, C. K., S. H. Jo and Y. Seo; "The Effect of Voidage on the CO<sub>2</sub> Sorption Capacity of K-Based Sorbent in a Dual Circulating Fluidized Bed Process," *J. Chem. Eng. Japan*, **41**, 691–694 (2008)
- Zhao, C., X. Chen, E. J. Anthony, X. Jiang, L. Duan, Y. Wu, W. Dong and C. Zhao; "Capturing CO<sub>2</sub> in Flue Gas from Fossil Fuel-Fired Power Plants Using Dry Regenerable Alkali Metal-Based Sorbent," *Prog. Energy Combust. Sci.*, **39**, 515–534 (2013)